Sensors and Actuators B 236 (2016) 350–357

Contents lists available at ScienceDirect

Sensors and Actuators B: Chemical

journal homepage: www.elsevier.com/locate/snb

Light irradiation enhanced triethylamine gas sensing materials based on ZnO/$ZnFe_2O_4$ composites

Shui-Ren Liu[a,b], Mei-Yu Guan[a,b], Xiao-Zhou Li[a,b], Ying Guo[a,b,*]

[a] State Key Laboratory of Chemical Resource Engineering, Beijing University of Chemical Technology, P.O. Box 98, Beijing, 100029, PR China
[b] Beijing Key Laboratory of Environmentally Harmful Chemical Analysis, Beijing University of Chemical Technology, Beijing, 100029, PR China

ARTICLE INFO

Article history:
Received 21 December 2015
Received in revised form 7 April 2016
Accepted 25 May 2016
Available online 27 May 2016

Keywords:
ZnO/$ZnFe_2O_4$ composites
Triethylamine
Gas sensor
Light irradiation

ABSTRACT

Light irradiation enhanced ZnO/$ZnFe_2O_4$ sensors for triethylamine gas detections have been reported in this paper. ZnO/$ZnFe_2O_4$ composites with a hexagonal nanostructure were synthesized by calcination of Zn, Fe layered double hydroxides (Zn_2Fe-LDH) at certain temperatures. Focusing on the general problem that the metal oxide gas sensors for triethylamine detection often have high working temperatures around 200 °C, the assistance approach of light irradiation has been conducted in our work. Under the light irradiation, the gas sensing measurement indicates that the sample calcined at 600 °C shows considerable response to triethylamine at the working temperature of 80 °C. For comparison, the introduction of light irradiation has lowered the working temperature markedly, which might have potential to monitor TEA in industrial production in the future.

1. Introduction

Triethylamine (TEA), a colorless liquid, has been widely used as solvent, curing agent, corrosion inhibitor, polymerization inhibitor, preservative, and synthetic dye [1–4]. Meanwhile, triethylamine is also one of the volatile organic compounds (VOCs) with a strong ammonia smell, which is flammable, combustible and pestilent as well. There is a strong irritant to the respiratory tract after inhalation due to its strong pungency, which can cause pulmonary edema and even death [4]. Therefore, it is very necessary to detect triethylamine momentarily. Nowadays, many analytical methods have been established for the determination of amines in water, including gas chromatography, electrochemistry analysis, immunoassays, thin-layer chromatography, high-performance liquid chromatography (HPLC) and so on [5]. However, most of these means are limited for the detection of volatile TEA gas for its non-portable character and often accompany with a high testing cost. For solving this problem, it is time for the portable gas sensors appear to construct the routine examination of TEA vapor. Recently, sensors based on metal oxide materials have been extensively investigated due to their high sensitivities, low costs, portability and simplicities of synthesis [6–8]. Actually, there already have a few gas sensors based on metal oxide semiconductors, which have shown high selectivity and rapid responses to TEA. For example, Liu et al. has reported that nano-sized LaF_3–CeO_2 shows high sensitivity and selectivity to TEA at 205 °C [4]. Zhang et al. has also reported that the SnO_2-ZnO nano composite sensor shows high and quick responses to TEA at 330 °C [9]. Although all the above sensors exhibit good responses towards TEA, their working temperatures are inevitably high. Obviously, it is dangerous to detect this flammable and combustible gas of TEA at high temperature of 200–300 °C. As we all know, at low working temperature like below 200 °C, metal oxide gas sensors often exhibit poor sensing ability or even show no response to target gas. To solve this problem, light-assisted gas sensor has attracted growing attentions because they can obtain higher response than that of classical heat-assisted gas sensor at low temperature with the help of light irradiation [10–12]. It has been proved that light irradiation may be an effective mean for metal oxide gas sensors to achieve low temperature detection characteristic.

As we all have known, the key part of sensor is sensing material. Layered double hydroxides (LDHs) are synthetic two dimensional nanostructured anionic clays with the general formula with the general formula $[M^{2+}_{1-x}M^{3+}_x(OH)_2]^{x+}(A^{n-})_{x/n}\cdot mH_2O$, where $M^{2+}$and M^{3+} are divalent and trivalent cations, respectively, x is equal to the ratio $M^{3+}/(M^{2+}+M^{3+})$ and A^{n-} represents the interlayer guest anions in the hydrated interlayer galleries [13,14]. Using LDHs as a source precursor, metal oxide composites can be obtained by roasting the layered nanosheets. The resulting products not only show high stability against sintering but also exhibit homogeneous

* Corresponding author at: State Key Laboratory of Chemical Resource Engineering, Beijing University of Chemical Technology, P.O. Box 98, Beijing, 100029, PR China.
E-mail addresses: guoying@mail.buct.edu.cn, guoyingbuct@gmail.com (Y. Guo).

http://dx.doi.org/10.1016/j.snb.2016.05.130
0925-4005/

dispersion between the elements, all of that have been supposed to be contributive to better gas sensing properties [15,16].

Herein, a strategy for producing ZnO/$ZnFe_2O_4$ composites with Zn_2Fe-LDH as a single source precursor has been presented. The gas sensors based on ZnO/$ZnFe_2O_4$ composites not only exhibit good gas sensing ability towards TEA as a traditional heat-assisted gas sensor at a higher working temperature between 200 and 300 °C, but also show considerably sensitivity and fast response/recovery speed towards TEA at a lower working temperature such as 80 °C with the help of light irradiation, which are proved to be potential light-assisted gas sensing materials in the field of TEA detection.

2. Experimental

2.1. Synthesis process

All the reagents were analytical grade and were used as received without further purification. The starting materials were $Zn(NO_3)_2{\cdot}6H_2O$ (99.0% purity from Guangfu Chemical Co., Ltd.), $Fe(NO_3)_3{\cdot}9H_2O$ (98.5% purity from Guangfu Chemical Co., Ltd.), Sodium dodecyl sulfate (SDS) (85% purity from Xilong Chemical Co., Ltd.) and NaOH (96.0% purity from Beijing chemical plant).

2.1.1. Preparation of Zn_2Fe-LDH precursor

The precursor Zn_2Fe-LDH with sodium dodecyl sulfate (SDS) as an interlayer guest anion was prepared following a classical co-precipitation method and a hydrothermal process. In a typical experiment, $Zn(NO_3)_2{\cdot}6H_2O$ (5.95 g, 0.02 mol), $Fe(NO_3)_3{\cdot}9H_2O$ (4.04 g, 0.01 mol) were dissolved in 15 ml deionized water to form a homogeneous solution. Afterwards, SDS (5.77 g, 0.02 mol) was introduced into the above solution, after vigorously stirring for one hour, a solution of NaOH (1 M) was added drop wise over 30 min to the above mixture until the pH of the slurry reached at 8. Another vigorously stirring for six hours was imposed to the slurry before it was transferred into a Teflon-line autoclave, after aging at 100 °C for 10 h. The product was separated by filtration, rinsed with distilled water several times, and then dried at 60 °C for 12 h in an oven.

2.1.2. Preparation of ZnO/$ZnFe_2O_4$ composites

The LDH precursors were calcined respectively at 600, 800, 1000 °C for 5 h in air with a rate of 2 °C min^{-1} in a muffle stove, and the resulting composite oxides were obtained, which were named as ZnO/$ZnFe_2O_4$-600, ZnO/$ZnFe_2O_4$-800 and ZnO/$ZnFe_2O_4$-1000, respectively.

2.2. Characterization

The crystalline phase of materials was examined using X-ray diffraction (XRD) characterizations on a Rigaku XRD-6000 diffractometer using Cu Kα radiation (λ = 0.15418 nm) at an accelerating voltage of 40 kV and current of 30 mA. Scanning electron microscopy (SEM) images were obtained using a Zeiss SUPRA 55 at 20 kV, with the surface of the samples coated with a thin platinum layer to avoid a charging effect. High-resolution transmission electron microscope (HRTEM) was recorded on a JEOL J-2100 to examine the morphologies, lattice fringes and crystal boundaries of the composites. The specific surface area was estimated using the Brunauer–Emmett–Teller (BET) equation based on the nitrogen adsorption isotherm obtained with a Micromeritics Gemini VII apparatus (Surface Area and Porosity System). The chemical surface's valence states of elements were performed using Thereto VGESCALAB 250 X-ray photoelectron spectroscopy (XPS) with all of the binding energy corrected by contaminant carbon (C 1s = 284.6 eV).

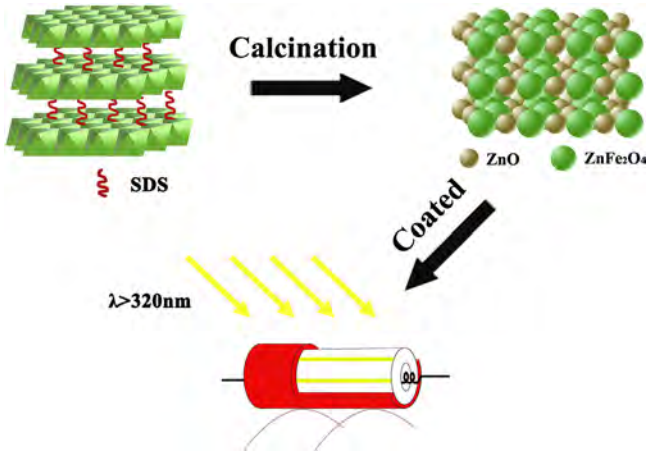

Fig. 1. Schematic illustration of gas sensor based on ZnO/$ZnFe_2O_4$ composites.

2.3. Gas sensing measurements

All gas sensing measurements were performed on a measuring system of chemical gas sensing-8 (CGS-8) from ELITE TECH. China. The metal oxide materials were grinded with a small amount of deionized water to form a paste, and then were evenly coated on alumina ceramic tube (as shown in Fig. 1). Two gold electrodes were printed on the ceramic tube with a gap of about 1 mm, each of which was connected with two platinum wires. A small Ni − Cr alloy coil was placed through the tube as a heater, and the working temperature can be controlled by adjusting the heating current. After aging at 80 mA for 24 h in air, the gas sensor can be used for preliminary measurement. The gas response (sensitivity) was designated as R_0/R_t, where R_0 was the sensor resistance in air (base resistance) and R_t was the sensor resistance at a certain time in the test. The time taken by the sensor to achieve 90% of the total resistance change in the case of adsorption and desorption was defined as the response and recovery time respectively.

The target gas or the interference gases were prepared by injecting the liquid into a container inside the chamber and evaporating it with a heater. A fan in the test chamber was used to make evaporated gas mixed evenly.

Photosensitive properties of the sensors were carried out by employing a mercury-xenon lamp with a power of 150 mW/cm^2 at λ > 320 nm. To avoid the effect of light irradiation cycles on the sensor application, the composites sensors were first irradiated with mercury-xenon lamp for 12 h prior to photosensitive measurements. Light irradiation enhanced gas sensing measurements were conducted as follows: Typically, the gas sensitive test was carried out in the instrument's chamber, which was coated with a light shielding paper except a circular breach to let the light pass through. For one cycle, the gas sensing element was placed in the instrument test bench until its resistance value reached stable, and then the light (150 mW/cm^2 at λ > 320 nm) was turned on. After an irradiation time of 300 s, the target gas was injected into the chamber. When the resistance value of the gas sensing element reached stable in the target gas, the light was removed and the chamber was opened to let the air in.

3. Results and discussion

3.1. Structural and morphological characteristics

Powder X-ray diffraction (XRD) was conducted to identify the composition and crystalline phase of the precursor. Fig. 2 shows the XRD patterns of Zn_2Fe-LDH precursor and its calcined products

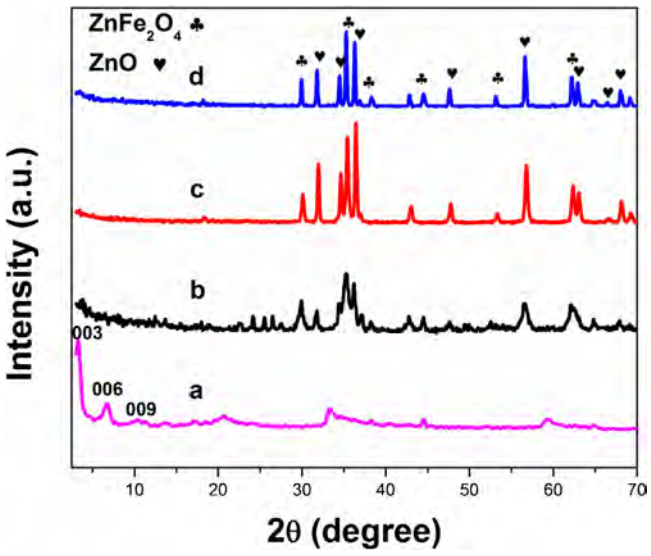

Fig. 2. XRD patterns of Zn_2Fe-LDH precursor (a) and its calcined products at 600 °C (b), 800 °C (c) and 1000 °C (d).

at three temperatures. The main diffraction peaks (003, 006, 009) observed in Fig. 2a are the typical symmetric (00l) lines of layered double hydroxide, corresponding to the basal spacing and higher order reflections [17]. The basal spacing calculated from the (003) reflection is 2.69 nm, which is much larger than that of the LDH with the intercalated anion of CO_3^{2-} (0.75 nm) [18]. As the calculated length of the SDS molecule is 21.3 Å and the layer thickness is about 4.8 Å, the sum of which basically coincides with the basal spacing of the layered material. It indicates that the sodium dodecyl sulfate was oriented perpendicularly in the gallery of LDH [19]. As shown in Fig. 2, the layered characteristic of the Zn_2Fe-LDH are replaced by the peaks of hexagonal ZnO phase (JCPDS Card No. 36-1451) and the cubic structure of $ZnFe_2O_4$ (JCPDS Card No. 22-1012) after calcined at three calcination temperatures. No extra diffraction peaks for other Fe related phases such as FeO, Fe_2O_3, and Fe_3O_4 are observed in the XRD patterns, indicating that all of the three calcined products are mainly composite oxides of ZnO and $ZnFe_2O_4$. The relative intensities of related signals grow stronger and sharper with the increase of calcination temperature, indicating the better crystallinity of the calcined products at higher temperatures.

The morphology images of Zn_2Fe-LDH precursor and the calcined products are observed by SEM. As shown in Fig. 3, we can clearly see that the lamellar structure of Zn_2Fe-LDH precursor (Fig. 3a) transformed into well-crystallized hexagonal crystals with high degree of order after calcination at 600 °C (Fig. 3b). The calcined products emerged a thicker crystals' thickness with the increase of calcination temperature and its morphology turned to round pie shape when the firing temperature rose to 800 °C (Fig. 3c) and 1000 °C (Fig. 3d).

As displayed in Fig. 4a, the typical TEM image of hexagonal nano sheets of $ZnO/ZnFe_2O_4$-600 is consistent with the morphology displayed from the scanning electron microscopy (Fig. 3b). The size of hexagonal nano sheets is average 15 nm. From the image of

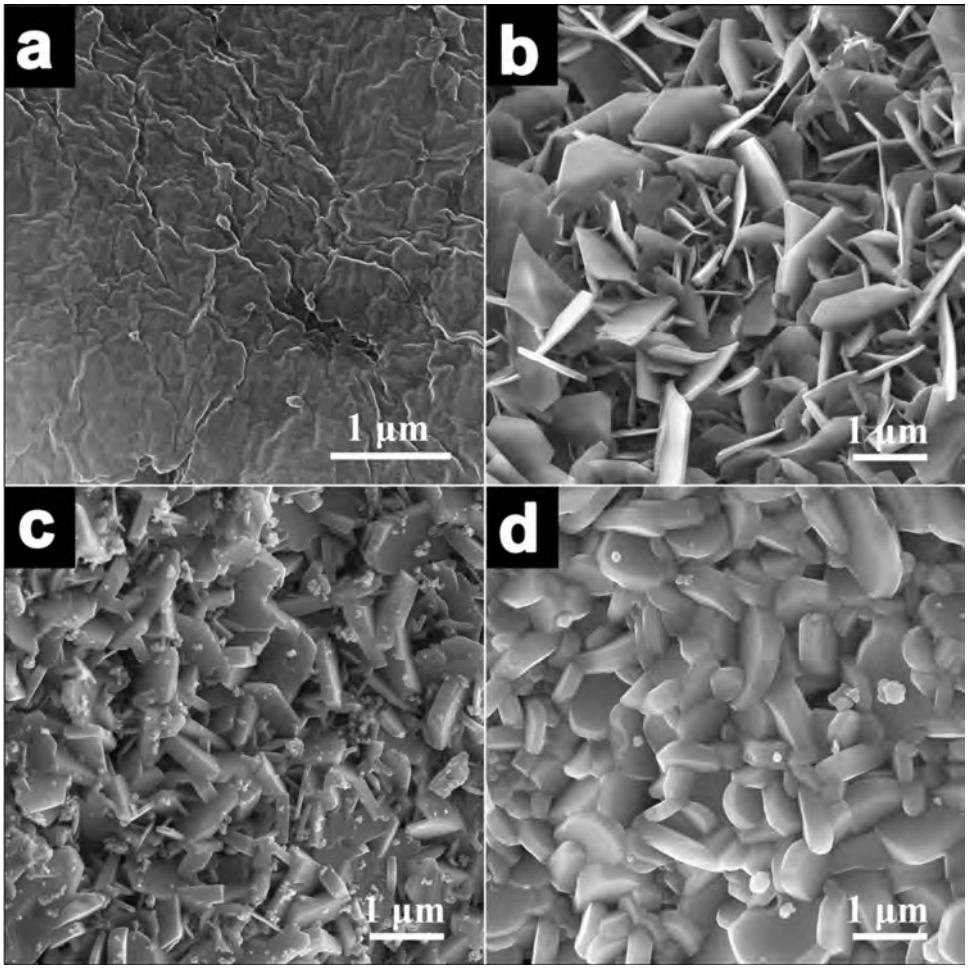

Fig. 3. Typical SEM images of Zn_2Fe-LDH precursor (a) and its calcined products at 600 °C (b), 800 °C (c) and 1000 °C (d).

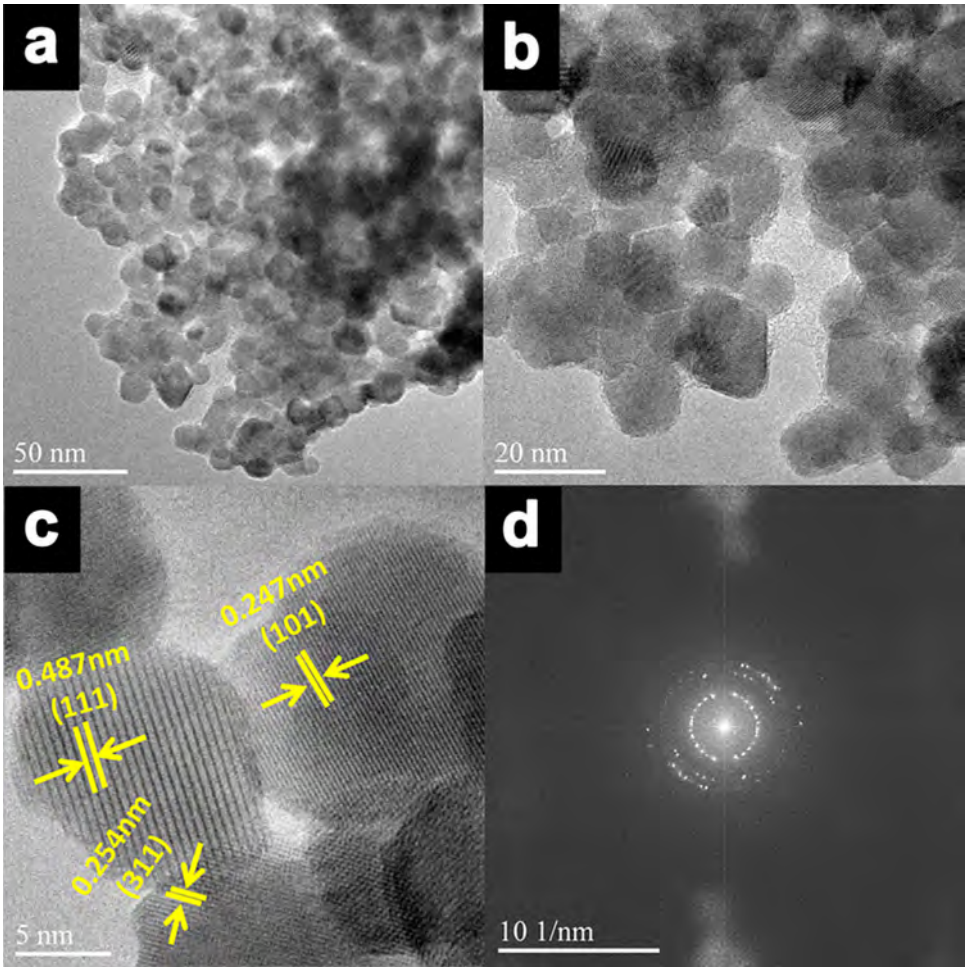

Fig. 4. Typical TEM images of $ZnO/ZnFe_2O_4$-600 (a, b), HRTEM image of $ZnO/ZnFe_2O_4$-600 (c) and the corresponding SAED pattern of $ZnO/ZnFe_2O_4$-600 (d).

HRTEM (Fig. 4b), the lattice fringes are clearly observed, such as the fringe spacing of 0.487 nm, 0.254 nm, 0.247 nm, which are consistent with the interplanar spacing of (111) and (311) planes of cubic structure of $ZnFe_2O_4$ (JCPDS Card No. 22-1012) and (311) planes of hexagonal ZnO (JCPDS Card No. 36-1451), respectively. Fig. 4c is the selected area electron diffraction (SAED) pattern of $ZnO/ZnFe_2O_4$-600, a series of diffraction rings can be clearly observed from it, which indicates that the $ZnO/ZnFe_2O_4$-600 nanosheets are polycrystalline. Obviously, the uniform distributed hexagonal crystals of ZnO and $ZnFe_2O_4$ are obtained successfully by calcination of LDH precursor.

To get more information about the chemical state and composition of the as-synthesized $ZnO/ZnFe_2O_4$ composites, XPS analysis was employed (Fig. S1), conforming the coexistence of Zn, Fe, and O in the composite. Major peaks observed in XPS spectra imply the Zn^{2+} and Fe^{3+}oxidation state in $ZnO/ZnFe_2O_4$ composites, which are in accordance with the references [19–21]. Therefore, the $ZnO/ZnFe_2O_4$ composites have been obtained successfully by one single source precursor.

3.2. Gas sensing properties

Since the operating temperature is a key parameter for a semiconductor oxide sensor to exert its sensing properties [22], the relationships between the responses and the operating temperature of the sensors were investigated. Fig. 5 shows the responses of three sensors based on $ZnO/ZnFe_2O_4$ composites to 100 ppm TEA under different operation temperatures. It can be seen that the response of $ZnO/ZnFe_2O_4$-600 sensor reaches its maximum sensing value of 28 at 240 °C, which is its optimal operating temperature. Similarly, the maximum response of $ZnO/ZnFe_2O_4$-800 and $ZnO/ZnFe_2O_4$-1000 sensors is 11 and 13 at 210 °C and 265 °C,

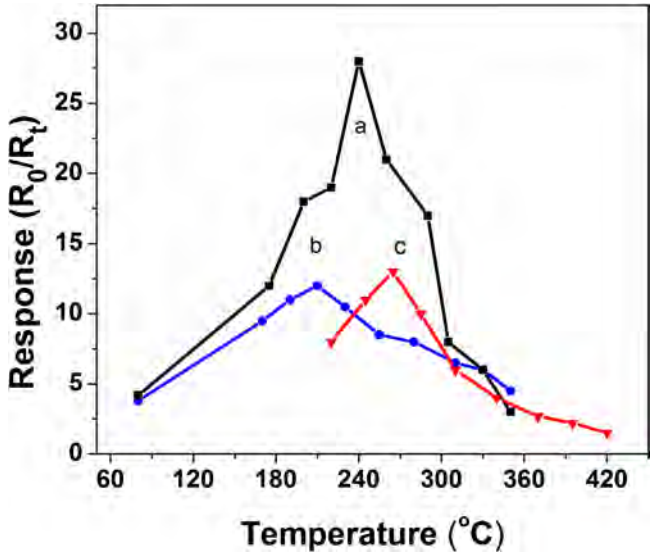

Fig. 5. Response of $ZnO/ZnFe_2O_4$-600 (a), $ZnO/ZnFe_2O_4$-800 (b) and $ZnO/ZnFe_2O_4$-1000 (c) to 100 ppm TEA at different operation temperatures.

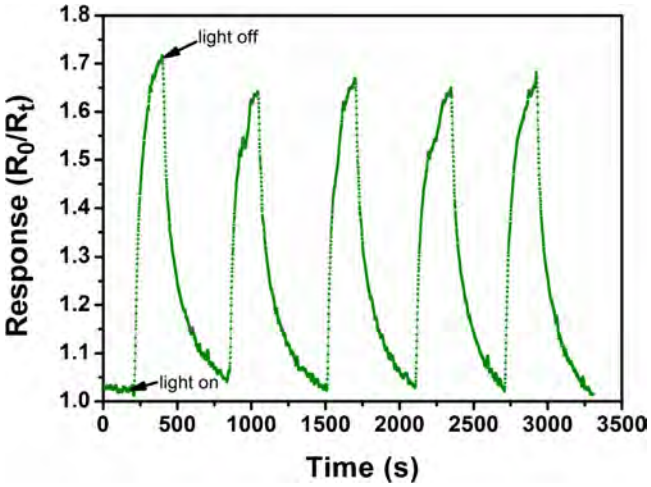

Fig. 6. Time-dependent photoresponse of ZnO/$ZnFe_2O_4$-600 measured by turning on and off the light with a λ > 320 nm and a power of 150 mW/cm^2 at 80 °C.

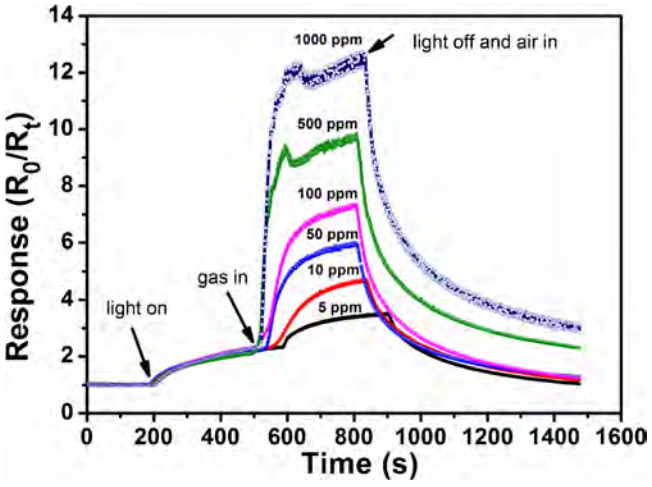

Fig. 7. Response-recovery curves of ZnO/$ZnFe_2O_4$-600 to different TEA concentrations under light irradiation at the working temperature of 80 °C.

respectively. Apparently, their maximal responses appear at different temperatures. Among the three composites, ZnO/$ZnFe_2O_4$-600 always has a highest response at the operation temperature range of 80 °C–340 °C, which should be attributed to the highest specific surface area. Normally, the smaller its grain size is, the higher specific surface area is. As indicated from the specific surface area of these three composites, the specific surface area of ZnO/$ZnFe_2O_4$-600 (59.9 m^2/g) is much larger than that of ZnO/$ZnFe_2O_4$-800 (17.7 m^2/g) and ZnO/$ZnFe_2O_4$-1000 (27.7 m^2/g). Thus the high specific surface causes high oxygen adsorption quantity, accompanying the high gas response of ZnO/$ZnFe_2O_4$-600 [23]. The larger specific surface, the more reactive sites will be provided for target gas, therefore ZnO/$ZnFe_2O_4$-600 presents a higher response than ZnO/$ZnFe_2O_4$-800 and ZnO/$ZnFe_2O_4$-1000. For comparison, ZnO-600 has been prepared by the same approach for the preparation of ZnO/$ZnFe_2O_4$-600 without adding ferric nitrate. However, the response of ZnO-600 to the same concentration of TEA is only 5 at the optimal working temperature (Fig. S2). Obviously, the introduction of $ZnFe_2O_4$ has significantly improved the gas-sensing properties of pure ZnO.

Nevertheless, it is noticed that when the working temperature falls below 100 °C, all of the three sensors show poor sensing ability with low response values and longer response time. Below 80 °C, there is almost no response for any of the three sensors. The lowest detection temperatures for ZnO/$ZnFe_2O_4$-600 and ZnO/$ZnFe_2O_4$-800 both are 80 °C and for ZnO/$ZnFe_2O_4$-1000 is 200 °C. Therefore, in spite of ZnO/$ZnFe_2O_4$-600 has wonderful gas sensing property to triethylamine vapor, it is obviously not safe for detection of TEA above 200 °C due to its flammable and explosive characteristic. Inspired by the reports that UV irradiation can make metal oxide sensors work at lower temperature with considerable response [24,25], the gas sensing properties of ZnO/$ZnFe_2O_4$-600 under light radiation at a working temperature around 80 °C were further studied.

Before the test of light assisted gas sensing, the photoresponse cycles of ZnO/$ZnFe_2O_4$ sensor were tested by turning on and off the light periodically, as shown in Fig. 6. It can be seen an increase of R_0/R_t, R_0 represents the initial resistance of the sensor in the air ambient and R_t represents the resistance of senor at certain time, which indicates the decrease of the sensor resistance (R_t) after the light was turned-on. The responses of the five cycles keep similar, which indicates the good reproducibility of ZnO/$ZnFe_2O_4$ sensor to light and the practicability of light assisted gas sensing. Compared with ZnO-600, ZnO/$ZnFe_2O_4$-600 sensor shows higher photoelectric response signal to the light, which means ZnO/$ZnFe_2O_4$-600 can utilize the visible light effectively (Fig. S3).

To evaluate TEA sensing performance of ZnO/$ZnFe_2O_4$ based sensor at low temperature, independent resistance change measurements were investigated at a working temperature of 80 °C. Before the chamber was injected with TEA liquid which was further evaporated into TEA gas, the chamber was irradiated under a light with λ > 320 nm and power of 150 mW/cm^2. Fig. 7 shows the typical response-recovery characteristics of the ZnO/$ZnFe_2O_4$-600 sensor to TEA with different concentrations from 5–1000 ppm. It can be seen a slow increase of R_0/R_t in Fig. 7, which indicates the decrease of the sensor resistance (R_t) after the light was turned-on. Normally, when the sensor is put into the air ambient, the oxygen molecules would grab the electrons from surface of the metal oxide and become the adsorbed O_2^-. After the target TEA gas is introduced into the chamber, the gas would react with the chemical surface adsorbed oxide ions and make the captured electrons transfer back to the sensor, which brought on the resistance (R_t) decrease and thus R_0/R_t continues to increase. Afterwards, the sensor's response (R_0/R_t) decreases to the initial value after the light is turned off and the air is poured in. The response values of ZnO/$ZnFe_2O_4$-600 sensor are approximately 3.4, 4.8, 6.0, 7.4, 10, and 12.8 to 5, 10, 50, 100, 500, and 1000 ppm of TEA respectively with response time of about 100 s.

Fig. 8 presents a more intuitive comparison between the response of ZnO/$ZnFe_2O_4$-600 sensor with and without light irradiation. Accordingly, under these same concentrations of TEA and without the assistance of light irradiation, the responses of ZnO/$ZnFe_2O_4$-600 sensor are only 1.5, 1.8, 4.0, 4.2, 6.2, and 7.3, respectively. Obviously, enhanced gas sensing properties could be clearly observed under light irradiation to all the TEA concentrations. Typically, the response value to 5 ppm TEA under light irradiation is 3.4, which is almost twice as that in the darkness (Fig. S4). Considering the response time, it takes around 300 s for the sensor responses to the TEA gas at the same operation temperature of 80 °C without light irradiation. Evidently, the light irradiation can effectively increase response values of R_0/R_t and shorten the response time of ZnO/$ZnFe_2O_4$-600 sensor to TEA.

To confirm the stability of the present ZnO/$ZnFe_2O_4$-600 TEA gas sensor, the gas sensing measurements of the sensor exposed to five continuous cycles to 50 ppm of TEA were carried out. As shown in Fig. 9, one can see a slow increase of the sensor response (R_0/R_t) once the light is turned-on. Another sharp increase can be also seen after the TEA gas is introduced into the chamber. The responses of the five cycles keep similar, which indicates the good reproducibil-

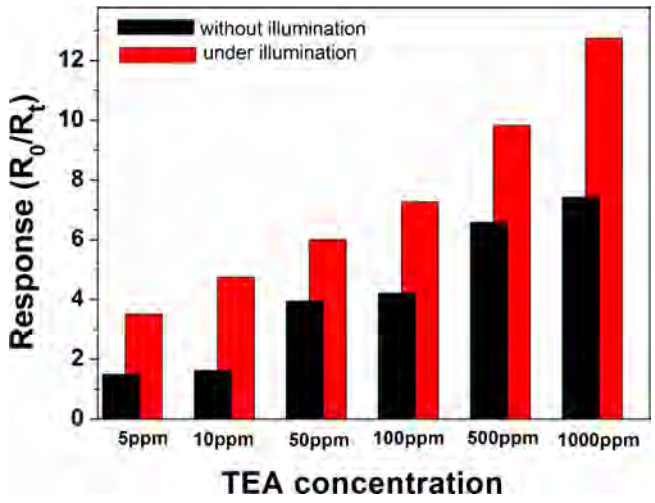

Fig. 8. Comparison of TEA responses of $ZnO/ZnFe_2O_4$-600 under and without light irradiation at 80 °C.

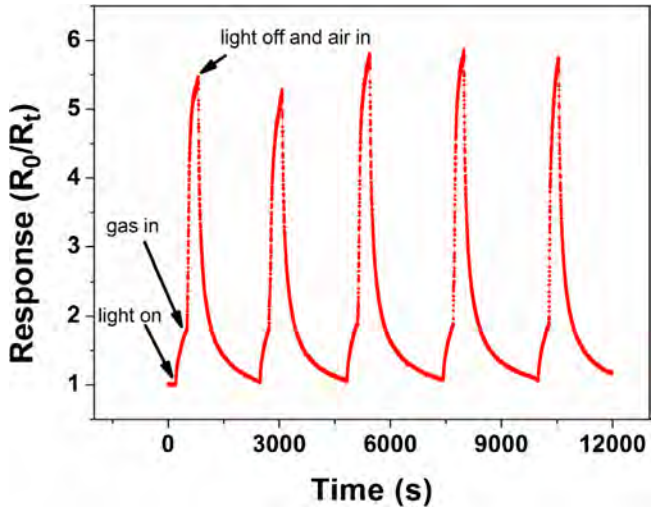

Fig. 9. Response-recovery cycles of $ZnO/ZnFe_2O_4$-600 to 50 ppm TEA under light irradiation at 80 °C.

ity of $ZnO/ZnFe_2O_4$-600 TEA gas sensor to the light as well as to the TEA gas. In addition, the same experiments were conducted six months later after the sensor was prepared. Five continuous cycles to 50 ppm of TEA were shown in Fig. S5, and the responses of $ZnO/ZnFe_2O_4$-600 sensor still floated around 6, which show the excellent long term stability of $ZnO/ZnFe_2O_4$-600 TEA gas sensor.

Selectivity is another important factor for practical application of a gas sensor, a sensor with good selectivity means one can detect target gas even in multicomponent gas environment [21]. Fig. 10a shows the response values of $ZnO/ZnFe_2O_4$-600 to thirteen vapors under the same concentration of 500 ppm at 240 °C. It is observed that $ZnO/ZnFe_2O_4$-600 shows a higher response to $(C_2H_5)_3N$ but less response to C_4H_9OH, C_3H_7OH, CH_3COCH_3, C_2H_5OH, NH_3 and so on. The response value of $ZnO/ZnFe_2O_4$-600 to TEA is almost twice as high as that to C_4H_9OH and 3.8 times to C_3H_7OH, not to mention other vapors. Fig. 10b depicts the selectivity of $ZnO/ZnFe_2O_4$-600 to 500 ppm vapors at low temperature of 80 °C under light irradiation. It is clear that $ZnO/ZnFe_2O_4$-600 almost shows no response to other gases except TEA, the response of $ZnO/ZnFe_2O_4$-600 to 500 ppm TEA is 12.7, almost 24 times as that to C_4H_9OH. Obviously, $ZnO/ZnFe_2O_4$-600 has better selectivity in detecting TEA under light irradiation even it is detected at such a low temperature of 80 °C. High selectivity means more accurately detection of target gas and better application prospect, which is practicable for a gas sensor.

3.3. Possible mechanism

It is well known that the chemical potential of oxygen is below the conduction band of ZnO and $ZnFe_2O_4$, which causes O_2^- forms on the surface through capturing electrons from n-type oxide semiconductor [26–29] at low temperature below 150 °C. Thus a high resistance depletion layer is formed near the surface of the $ZnO/ZnFe_2O_4$ composites in air. Continues with the light irradiation, the target gas is introduced into the test chamber and reacts with the adsorbed oxygen ions on the surface of $ZnO/ZnFe_2O_4$ composites as follows:

$$2Et_2N{-}CH_2{-}CH_3(ads) + O_2^-(ads) \rightarrow 2Et_2N{-}CH{=}CH_2 + 2H_2O + e^- [30, 31]$$

At the same time, the electrons trapped by the adsorbed oxygen molecules transfer back to the conduction band, which induces a great thinning of depletion layer (as shown in Fig. 11) and a decrease in resistance of $ZnO/ZnFe_2O_4$ composites, thus a high response of R_0/R_t to the target gas is observed.

The adsorption type of oxygen molecules is physisorption which is quite weak at low operating temperature, therefore low responses are observed without light irradiation. The high response under light irradiation may be due to the enhanced activity of

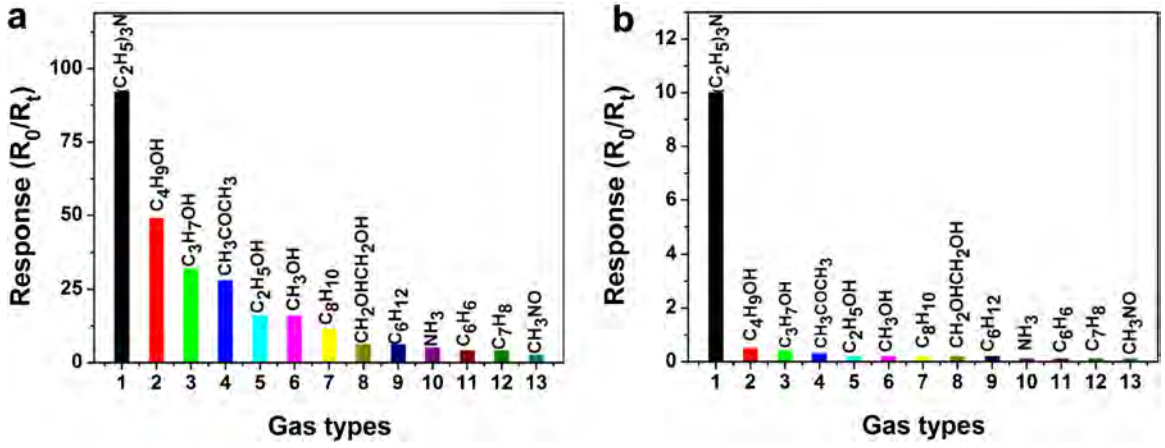

Fig. 10. Selectivity of $ZnO/ZnFe_2O_4$-600 to 500 ppm vapors at 240 °C without light irradiation (a) and at 80 °C under light irradiation (b).

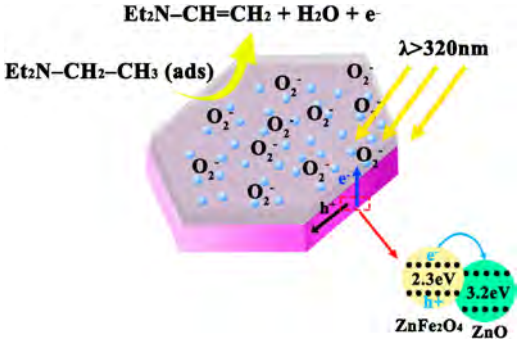

Fig. 11. Schematic illustration of sensing mechanism of the ZnO/$ZnFe_2O_4$-600 sensor.

adsorbed oxygen molecules during the light irradiation, which shift the equilibrium of the reactions and facilitate a higher reaction rate [32,33] between TEA and the adsorbed oxygen molecules. In addition, illumination often influences the gas adsorption rate and the activation energy [33,34], thus, the responses of the ZnO/$ZnFe_2O_4$ sensor for TEA are greatly improved.

4. Conclusions

The synthesis of ZnO/$ZnFe_2O_4$ composites with Zn_2Fe-LDH as a single source precursor has been described. ZnO/$ZnFe_2O_4$ composites show good response to TEA at 240 °C and weak response to TEA at low temperature of 80 °C. Enhanced sensing properties with respect to TEA have been observed through the exciting of light irradiation. Typically, the sample calcined at 600 °C performs impressive TEA sensing behaviors with advantages of good sensitivity, satisfactory stability and high selectivity. The present finding clearly demonstrates that light excitation is greatly helpful to improve the sensitivity of metal oxide gas sensors and lower the operating temperature, which might have potential to monitor TEA in industrial production in the future.

Acknowledgments

This work was supported by the National Natural Science Foundation of China (NSFC 51472021), the Scientific Research Foundation for the Returned Overseas Chinese Scholars, State Education Ministry (LXJJ201302), the Fundamental Research Funds for the Central Universities (YS1406) and Program for Changjiang Scholars and Innovative Research Team in University (IRT1205).

Appendix A. Supplementary data

Supplementary data associated with this article can be found, in the online version, at http://dx.doi.org/10.1016/j.snb.2016.05.130.

References

[1] M. Bietti, M. Salamone, Kinetic solvent effects on hydrogen abstraction reactions from carbon by the cumyloxyl radical. The role of hydrogen bonding, Org. Lett. 12 (2010) 3654–3657.
[2] J.R. De la Fuente, C. Jullian, C. Saitz, V. Neira, Unexpected formation of 1-diethylaminobutadiene in photosensitized oxidation of triethylamine induced by 2,3-dihydro-oxoisoaporphine dyes. A ^{1}H NMR and isotopic exchange study, J. Org. Chem. 70 (2005) 8712–8716.
[3] S.A. Lermontov, T.N. Velikokhatko, S.I. Zzvorin, Triethylamine as an effective catalyst for the reaction of CO_2 with epichlorohydrin, Russ. Chem. Bull. 47 (1998) 1405–1406.
[4] L. Xu, H. Song, J. Hu, Y. Lv, K. Xu, A cataluminescence gas sensor for triethylamine based on nanosized LaF_3–CeO_2, Sens. Actuators B: Chem. 169 (2012) 261–266.
[5] E. Filippoa, D. Manno, A. Buccolleri, A. Serraa, Green synthesis of sucralose-capped silver nanoparticles for fast colorimetric triethylamine detection, Sens. Actuators B: Chem. 178 (2013) 1–9.
[6] C. Wang, X. Cheng, X. Zhou, P. Sun, X. Hu, K. Shimanoe, G. Lu, N. Yamazoe, Hierarchical α-Fe_2O_3/NiO composites with a hollow structure for a gas sensor, ACS Appl. Mater. Interfaces 6 (2014) 12031–12037.
[7] Z. Chen, M. Cao, C. Hu, Novel Zn_2SnO_4 hierarchical nanostructures and their gas sensing properties toward ethanol, J. Phys. Chem. C 115 (2011) 5522–5529.
[8] M. Guan, D. Xu, Y. Song, Y. Guo, ZnO/$ZnAl_2O_4$ prepared by calcination of ZnAl layered double hydroxides for ethanol sensing, Sens. Actuators B: Chem 188 (2013) 1148–1154.
[9] W. Zhang, W.D. Zhang, Fabrication of SnO_2–ZnO nanocomposite sensor for selective sensing of trimethylamine and the freshness of fishes, Sens. Actuators B: Chem. 134 (2008) 403–408.
[10] L. Peng, J. Zhai, D. Wang, Y. Zhang, P. Wang, Q. Zhao, T. Xie, Size- and photoelectric characteristics-dependent formaldehyde sensitivity of ZnO irradiated with UV light, Sens. Actuators B: Chem. 148 (2010) 66–73.
[11] L. Peng, Q. Zhao, D. Wang, J. Zhai, P. Wang, S. Pang, T. Xie, Ultraviolet-assisted gas sensing: a potential formaldehyde detection approach at room temperature based on zinc oxide nanorods, Sens. Actuators B: Chem. 136 (2009) 80–85.
[12] L. Peng, T. Xie, M. Yang, P. Wang, D. Wang, Light induced enhancing gas sensitivity of copper-doped zinc oxide at room temperature, Sens. Actuators B: Chem 131 (2008) 660–664.
[13] Steven P. Newman, W. Jones, Synthesis, characterization and applications of layered double hydroxides containing organic guests, New J. Chem. (1998) 105–115.
[14] L. Zhang, F. Li, D. Evans, X. Duan, Structure and surface characteristics of Cu-based composite metal oxides derived from layered double hydroxides, Mater. Chem. Phys. 87 (2004) 402–410.
[15] N. Barsan, U. Weimar, Conduction model of metal oxide gas sensors, J.Electroceram. 7 (2001) 143–167.
[16] S. Lenaerts, J. Roggen, G. Maes, FT-IR characterization of tin dioxide gas sensor materials under working conditions, Spectrochim. Acta Part A 51A (1995) 883–894.
[17] N. Kang, D. Wang, B. Kutlu, P. Zhao, A. Leuteritz, U. Wagenknecht, G. Heinrich, A new approach to reducing the flammability of Layered Double Hydroxide (LDH)-based polymer composites: preparation and characterization of dye structure-intercalated LDH and its effect on the flammability of polypropylene-grafted maleic anhydride/d-LDH composites, ACS Appl. Mater. Interface 5 (2013) 991–8997.
[18] J. He, B. Li, Multiple effects of dodecanesulfonate in the crystal growth control and morphosynthesis of Layered Double Hydroxides, J. Phys. Chem. C 112 (2008) 10909–10917.
[19] T. Yamashita, P. Hayes, Analysis of XPS spectra of Fe^{2+} and Fe^{3+} ions in oxide materials, Appl. Surf. Sci. 254 (2008) 2441–2449.
[20] X. Liu, J. Zhang, L. Wang, T. Yang, X. Guo, S. Wu, S. Wang, 3D hierarchically porous ZnO structures and their functionalization by Au nanoparticles for gas sensors, J. Mater. Chem. 21 (2011) 349–356.
[21] S. Wang, J. Yang, X. Gao, H. Zhang, Y. Wang, Z. Zhu, Spinel $ZnFe_2O_4$ nanoparticle-decorated rod-like ZnO nanoheterostructures for enhanced gas sensing performances, RSC Adv. 5 (2015) 10048–10057.
[22] Q. Xu, D. Xua, M. Guan, Y. Guo, Q. Qi, G. Li, ZnO/Al_2O_3/CeO_2 composite with enhanced gas sensing performance, Sens. Actuators B: Chem. 177 (2013) 1134–1141.
[23] J. Xu, Q. Pan, Y. Shun, Z. Tian, Grain size control and gas sensing properties of ZnO gas sensor, Sens. Actuators B: Chem. 66 (2000) 277–279.
[24] E. Comini, G. Faglia, G. Sberveglieri, UV light activation of tin oxide thin films for NO_2 sensing at low temperatures, Sens. Actuators B: Chem. 78 (2001) 73–77.
[25] S. Mishra, C. Ghanshyama, N. Rama, R. Bajpai, R. Bedi, Detection mechanism of metal oxide gas sensor under UV radiation, Sens. Actuators B: Chem. 97 (2004) 387–390.
[26] A.A. Tahir, K.G.U. Wijayantha, Photoelectrochemical water splitting at nanostructured $ZnFe_2O_4$ electrodes, J. Photochem. Photobiol. A 216 (2010) 119–125.
[27] C. Soci, A. Zhang, B. Xiang, S.A. Dayeh, D.P.R. Aplin, J. Park, X.Y. Bao, Y. Lo, D. Wang, ZnO nanowire UV photodetectors with high internal gain, Nano Lett. 7 (2007) 1003–1009.
[28] X. Guo, H. Zhu, Q. Li, Visible-light-driven photocatalytic properties of ZnO/$ZnFe_2O_4$ core/shell nano cablearrays, Appl. Catal. B 160–161 (2014) 408–414.
[29] J. Li, Z. Liu, Z. Zhu, Enhanced photocatalytic activity in $ZnFe_2O_4$-ZnO-Ag_3PO_4 hollow nanospheres through the cascadal electron transfer with magnetical separation, J. Alloys Compd. 636 (2015) 229–233.
[30] L. Xu, H. Song, J. Hu, Y. Lv, K. Xu, A cataluminescence gas sensor for triethylamine based on nanosized LaF_3–CeO_2, Sens. Actuators B: Chem. 169 (2012) 261–266.
[31] L.L. Sui, Y.M. Xu, X.F. Zhang, X.L. Cheng, S. Gao, H. Zhao, Z. Cai, L.H. Huo, Construction of three-dimensional flower-like α-MoO_3 with hierarchical structure for highly selective triethylamine sensor, Sens. Actuators B: Chem. 208 (2015) 404–414.
[32] C.H. Han, D.W. Hong, S.D. Han, J. Gwak, K.C. Singh, Catalytic combustion type hydrogen gas sensor using TiO_2 and UV-LED, Sens. Actuators B: Chem. 125 (2007) 224–228.

[33] L. Peng, T.F. Xie, M. Yang, P. Wang, D. Xu, S. Pang, D.J. Wang, Light induced enhancing gas sensitivity of copper-doped zinc oxide at room temperature, Sens. Actuators B: Chem. 131 (2008) 660–664.
[34] E. Comini, A. Cristalli, G. Faglia, G. Sberveglieri, Light enhanced gas sensing properties of indium oxide and tin dioxide sensors, Sens. Actuators B: Chem. 65 (2000) 260–263.

Biographies

Shui-Ren Liu is a master student in Dr. Guo's group, in the College of Science, Beijing University of Chemical Technology, China. His project is focusing on the preparation and characterization of composite oxides for room temperature application.

Mei-Yu Guan was a master student in Dr. Guo's group and has obtained her Master degree with the work on the preparation and characterization of gas sensing materials. Now she is a technician in the College of Science, Beijing University of Chemical Technology, China.

Xiao-Zhou Li is a master student in Dr. Guo's group, in the College of Science, Beijing University of Chemical Technology, China. His project is focusing on the preparation and characterization of sensing materials, including polymer type sensing materials.

Dr. Ying Guo is an Associate Professor at State Key Laboratory of Chemical Resource Engineering, Beijing University of Chemical Technology, China. Her work mainly focuses on the inorganic/organic nanocomposites in gas sensing, supramolecular assemblies based on intercalated chemistry etc.